



**HAL**  
open science

## Cleavage of Na<sup>+</sup> channels by calpain increases persistent Na<sup>+</sup> current and promotes spasticity after spinal cord injury

Cécile Brocard, Vanessa Plantier, Pascale Boulenguez, Sylvie Liabeuf, Mouloud Bouhadfane, Annelise Viallat-Lieutaud, Laurent Vinay, Frédéric Brocard

### ► To cite this version:

Cécile Brocard, Vanessa Plantier, Pascale Boulenguez, Sylvie Liabeuf, Mouloud Bouhadfane, et al.. Cleavage of Na<sup>+</sup> channels by calpain increases persistent Na<sup>+</sup> current and promotes spasticity after spinal cord injury. *Nature Medicine*, 2016, 22 (4), pp.404-411. 10.1038/nm.4061 . hal-01463798

**HAL Id: hal-01463798**

**<https://amu.hal.science/hal-01463798>**

Submitted on 16 Feb 2017

**HAL** is a multi-disciplinary open access archive for the deposit and dissemination of scientific research documents, whether they are published or not. The documents may come from teaching and research institutions in France or abroad, or from public or private research centers.

L'archive ouverte pluridisciplinaire **HAL**, est destinée au dépôt et à la diffusion de documents scientifiques de niveau recherche, publiés ou non, émanant des établissements d'enseignement et de recherche français ou étrangers, des laboratoires publics ou privés.



Distributed under a Creative Commons Attribution - NonCommercial - NoDerivatives 4.0 International License

# Cleavage of Na<sup>+</sup> channels by calpain increases persistent Na<sup>+</sup> current and promotes spasticity after spinal cord injury

Cécile Brocard<sup>1,2</sup>, Vanessa Plantier<sup>1,2</sup>, Pascale Boulenguez<sup>1,2</sup>, Sylvie Liabeuf<sup>1</sup>, Mouloud Bouhadfane<sup>1</sup>, Annelise Viallat-Lieutaud<sup>1</sup>, Laurent Vinay<sup>1</sup> & Frédéric Brocard<sup>1</sup>

Upregulation of the persistent sodium current ( $I_{NaP}$ ) in motoneurons contributes to the development of spasticity after spinal cord injury (SCI). We investigated the mechanisms that regulate  $I_{NaP}$  and observed elevated expression of voltage-gated sodium (Nav) 1.6 channels in spinal lumbar motoneurons of adult rats with SCI. Furthermore, immunoblots revealed a proteolysis of Nav channels, and biochemical assays identified calpain as the main proteolytic factor. Calpain-dependent cleavage of Nav channels after neonatal SCI was associated with an upregulation of  $I_{NaP}$  in motoneurons. Similarly, the calpain-dependent cleavage of Nav1.6 channels expressed in human embryonic kidney (HEK) 293 cells caused the upregulation of  $I_{NaP}$ . The pharmacological inhibition of calpain activity by MDL28170 reduced the cleavage of Nav channels,  $I_{NaP}$  in motoneurons and spasticity in rats with SCI. Similarly, the blockade of  $I_{NaP}$  by riluzole alleviated spasticity. This study demonstrates that Nav channel expression in lumbar motoneurons is altered after SCI, and it shows a tight relationship between the calpain-dependent proteolysis of Nav1.6 channels, the upregulation of  $I_{NaP}$  and spasticity.

Spasticity, a common debilitating complication in people with spinal cord injury (SCI), is characterized by a velocity-dependent increase in the tonic stretch reflex and spasms<sup>1</sup>. It is primarily attributed to a reduction in postsynaptic inhibition and an increase in the excitability of motoneurons below the lesion<sup>2</sup>. Although disinhibition is related to a dysregulation of chloride homeostasis<sup>3</sup>, the mechanisms that cause motoneuron hyperexcitability are not yet fully understood. In the healthy spinal cord, the excitability of motoneurons is set by brainstem-derived serotonin (5-hydroxytryptamine (5-HT)). The activation of 5-HT type 2 receptors (5-HT<sub>2</sub>) facilitates voltage-gated persistent calcium and sodium currents<sup>4,5</sup> (persistent inward currents, or PICs). These PICs considerably amplify the activity of brief synaptic excitatory inputs, which enables sustained muscle contractions<sup>6</sup>. PICs are reduced early after SCI<sup>7</sup> as compared to those in healthy spinal cords, but slowly recover within weeks, leading to excessive motoneuron activity that is characterized by the plateau potentials associated with muscle spasms<sup>8,9</sup>. The upregulation of Ca<sup>2+</sup> PICs in the chronic phase after the injury is due to the increased expression of 5-HT subtype 2C receptors (5-HT<sub>2C</sub>), which become constitutively active<sup>10</sup>. However, a major question that remains is how the Na<sup>+</sup> PIC ( $I_{NaP}$ )—a key conductance of the locomotor network<sup>11–14</sup> that drives plateau potentials in motoneurons<sup>15</sup>—is upregulated. In adult rats, spinal cord neurons express mRNA encoding five  $\alpha$ -subunits of sodium channels (Nav1.1, Nav1.2, Nav1.3, Nav1.6 and Nav1.7)<sup>16</sup>, but the main  $\alpha$ -subunits in spinal motoneurons are Nav1.1 and Nav1.6 (ref. 17). We demonstrate here that the upregulation of  $I_{NaP}$  after SCI is accompanied by a proteolytic cleavage of the  $\alpha$ -subunit of Nav channels. We further show that calpains, a family of intracellular calcium-dependent

cysteine proteases<sup>18</sup>, are responsible for the cleavage of Nav1.6 channels. Our results open new therapeutic avenues, given that blocking either  $I_{NaP}$  or the activity of calpain reduces spasticity.

## RESULTS

### Upregulation of Nav1.6 $\alpha$ -subunit expression after SCI

We tested whether abnormal expression of Nav channels accounts for the upregulation of  $I_{NaP}$  after SCI. To model SCI in rodents, we carried out a complete transection at the T8–T9 level in adult female rats to avoid regeneration of the supraspinal tracts. At 15 d, 30 d and 60 d after SCI or sham surgery, we performed immunohistochemistry in lumbar segments L4–L5 (caudal to the lesion) to analyze the expression of the two main Nav  $\alpha$ -subunits that are present in motoneurons (Nav1.1 and Nav1.6 (ref. 17)). A pan-Nav antibody that recognizes all Nav1 isoforms strongly stained axon initial segments (AISs) of motoneurons in both sham-operated and SCI rats (Fig. 1a). Although the Nav1.1  $\alpha$ -subunit was hardly detectable (Supplementary Fig. 1a), Nav1.6-specific immunolabeling largely overlapped the pan-staining (Fig. 1a, middle and right). The intensity of Nav immunostaining revealed by both the pan-Nav and the Nav1.6 antibodies was higher in motoneurons after SCI than in sham-operated controls as early as 15 d after SCI ( $P < 0.001$ ; Fig. 1a–c). Conversely, the Nav1.6-specific immunostaining in the AIS segments of Renshaw cells did not change after SCI ( $P > 0.05$ ; Supplementary Fig. 1b,c).

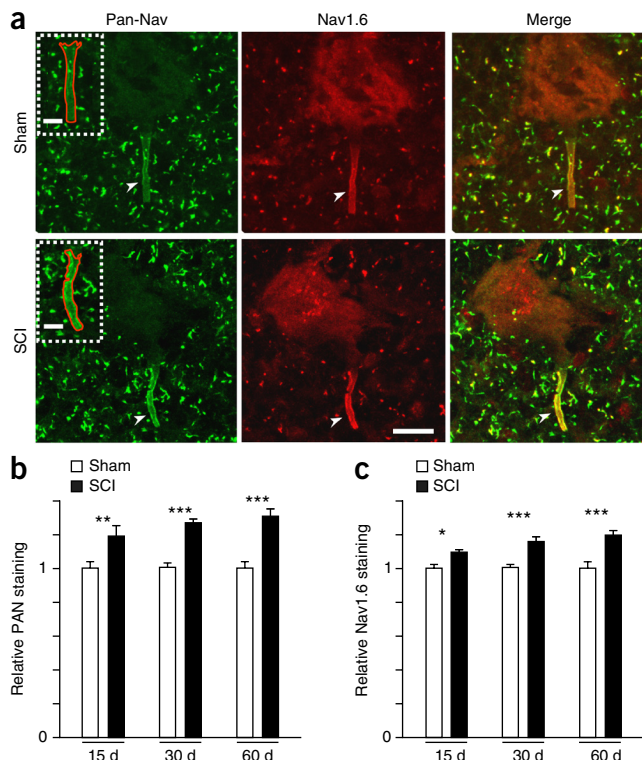
### Calpain mediates proteolysis of Nav1.6 channels after SCI

To confirm the changes in Nav expression after SCI, we performed western blots on the membrane fractions isolated from the lumbar

<sup>1</sup>Team P3M, Institut de Neurosciences de la Timone, UMR7289, Aix-Marseille Université and Centre National de la Recherche Scientifique (CNRS), Marseille, France. <sup>2</sup>These authors contributed equally to this work. Correspondence should be addressed to F.B. (frederic.brocard@univ-amu.fr).

Received 13 May 2015; accepted 8 February 2016; published online 14 March 2016; doi:10.1038/nm.4061

**Figure 1** Upregulation of motoneuron AIS Nav  $\alpha$ -subunits after SCI. (a) Example single optical sections showing immunostaining of Nav  $\alpha$ -subunits (left, pan-Nav antibody; middle, Nav1.6 antibody; right, merged images) in AISs (arrowheads) of lumbar motoneurons (L4–L5) in sham-operated (top) and rats with SCI (bottom; 30 d after SCI). The insets illustrate higher magnification of the pan-Nav immunoreactive AISs indicated by the arrowheads; red border marks the region used to analyze Nav staining intensity. Scale bars, 20  $\mu$ m (main images); 5  $\mu$ m (insets). (b,c) Relative immunostaining intensities obtained for pan-Nav (b) and Nav1.6 (c) antibodies in sham-operated (white) and rats with SCI (black), normalized to sham-operated controls at different time points after SCI.  $n = 51$  cells each from three rats per group (sham-operated and SCI) at 15 d; 52 cells each from four rats per group at 30 d; and 52 cells each from four rats per group at 60 d. Data are mean  $\pm$  s.e.m. \* $P < 0.05$ , \*\* $P < 0.01$ , \*\*\* $P < 0.001$  comparing sham-operated to SCI groups; two-way analysis of variance (ANOVA), Bonferroni's *post hoc* test for all panels.



spinal cord. The pan-Nav antibody revealed a prominent  $\sim$ 250-kDa band consistent with the full-length  $\alpha$ -subunits of Nav<sup>19</sup> (Fig. 2a). Although this band was unaffected by SCI, a distinct  $\sim$ 120-kDa band increased ( $P < 0.001$ ; Fig. 2a,b), such that the total amount of Nav channels at the membrane was higher in SCI samples than in sham-operated controls ( $P < 0.05$ ; Fig. 2b). In sham-operated rats 15–60 d after surgery, the  $\sim$ 120-kDa band represented a smaller proportion of total Nav protein relative to the  $\sim$ 250-kDa band ( $P < 0.001$ ; Fig. 2c), whereas in rats with SCI, the  $\sim$ 120-kDa and  $\sim$ 250-kDa bands were found to represent roughly equal proportions of total Nav protein ( $P > 0.05$ ; Fig. 2c). The expression of the neuronal microtubule element  $\beta$ -tubulin III, which was used as an internal control, did not change after SCI (Fig. 2b).

We then investigated Nav proteolysis in adult rat spinal cord homogenates. In Ca<sup>2+</sup>-chelated saline (5 mM ethylenediaminetetraacetic acid (EDTA)), homogenates revealed a single  $\sim$ 250-kDa band (Fig. 2d, left column). The addition of calcium (10 mM) in homogenates generated a  $\sim$ 120-kDa second band similar to that observed *in vivo* after

SCI (Fig. 2d, middle), which suggests the contribution of a cytosolic Ca<sup>2+</sup>-dependent protease. A pretreatment of homogenates with MDL28170, a widely used calpain inhibitor<sup>20,21</sup>, prevented the formation of this second band (Fig. 2d, right). Conversely, the addition of calpain progressively and dose-dependently reduced the  $\sim$ 250-kDa band and increased the  $\sim$ 120-kDa band corresponding to the cleaved

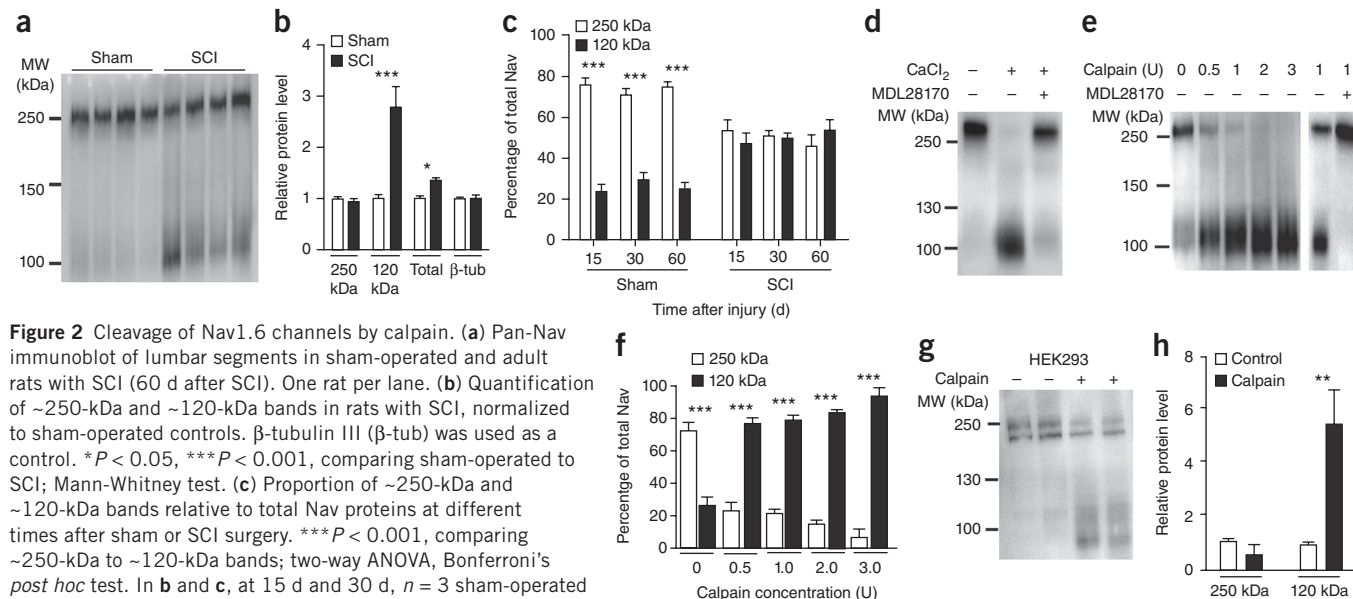


**Figure 2** Cleavage of Nav1.6 channels by calpain. (a) Pan-Nav immunoblot of lumbar segments in sham-operated and adult rats with SCI (60 d after SCI). One rat per lane. (b) Quantification of  $\sim$ 250-kDa and  $\sim$ 120-kDa bands in rats with SCI, normalized to sham-operated controls.  $\beta$ -tubulin III ( $\beta$ -tub) was used as a control. \* $P < 0.05$ , \*\*\* $P < 0.001$ , comparing sham-operated to SCI; Mann-Whitney test. (c) Proportion of  $\sim$ 250-kDa and  $\sim$ 120-kDa bands relative to total Nav proteins at different times after sham or SCI surgery. \*\*\* $P < 0.001$ , comparing  $\sim$ 250-kDa to  $\sim$ 120-kDa bands; two-way ANOVA, Bonferroni's *post hoc* test. In b and c, at 15 d and 30 d,  $n = 3$  sham-operated and  $n = 5$  rats with SCI; at 60 d,  $n = 4$  rats in each group.

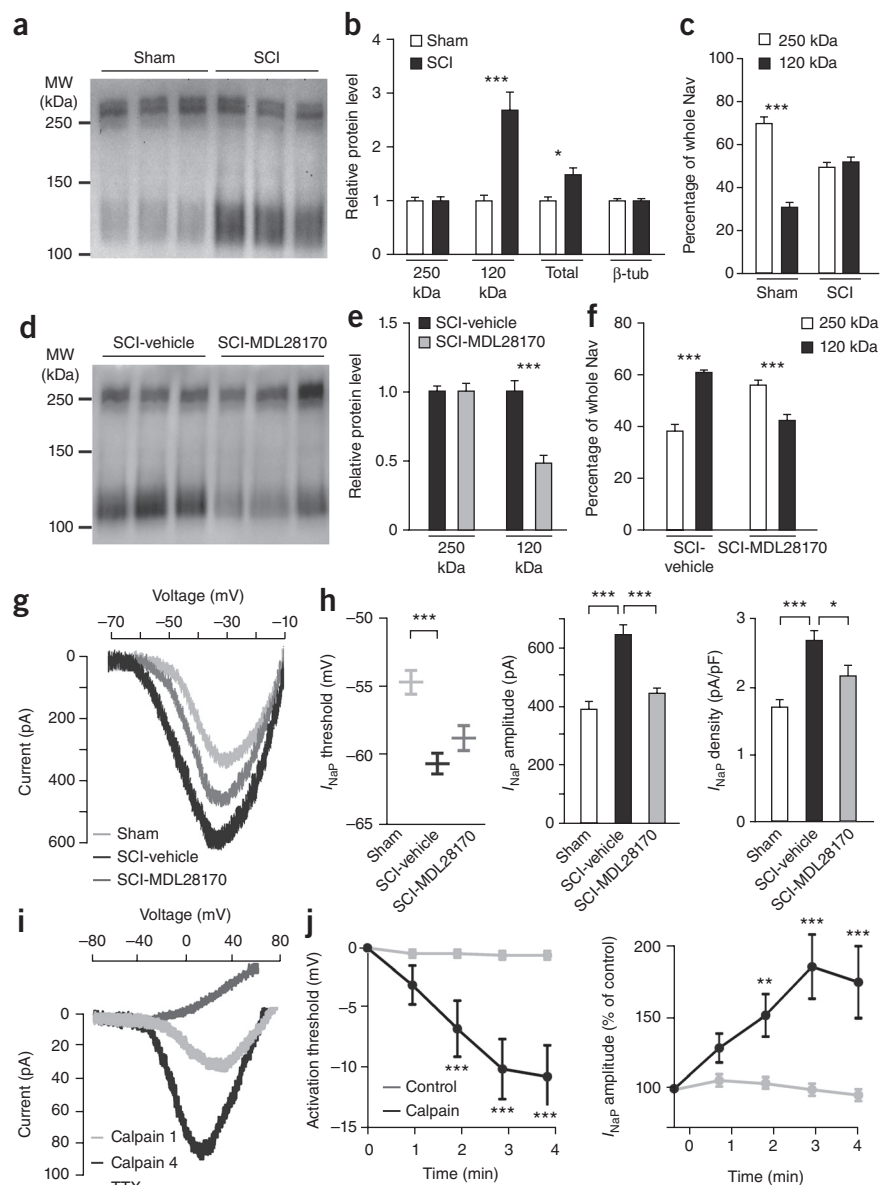
(d,e) Pan-Nav immunoblot of intact adult rat spinal cord homogenate incubated with Ca<sup>2+</sup> and/or MDL28170 (30  $\mu$ M; d), with increasing concentrations of calpain alone (0–3 U, left lanes in e), or with calpain (1 U) and MDL28170 (30  $\mu$ M, right lanes in e). (f) Quantification of  $\sim$ 250-kDa and  $\sim$ 120-kDa bands relative to total Nav protein (0 U,  $n = 8$ ; 0.5 U,  $n = 6$ ; 1 U,  $n = 2$ ; 2 U,  $n = 4$ ; 3 U,  $n = 2$ ;  $n$  replicates from four rats). \*\*\* $P < 0.001$ , comparing  $\sim$ 250-kDa to  $\sim$ 120-kDa bands; two-way ANOVA, Bonferroni's *post hoc* test. (g) Pan-Nav immunoblot of HEK293 Nav1.6-expressing cells with or without calpain (1 U). (h) Quantification of  $\sim$ 250-kDa and  $\sim$ 120-kDa bands in calpain-treated culture, normalized to untreated culture (0 U,  $n = 4$ ; 1 U,  $n = 6$ ;  $n$  replicates from two cultures). \*\* $P < 0.01$ ; Mann-Whitney test. Data are mean  $\pm$  s.e.m. for all panels.

**Figure 3** Calpain inhibition prevents the cleavage of Nav channels and the  $I_{NaP}$  increase after SCI. **(a)** Pan-Nav immunoblot of lumbar segments in sham-operated and neonatal rats with SCI (7 d after SCI). One rat per lane. **(b)** Quantification of ~250-kDa and ~120-kDa bands in rats with SCI ( $n = 11$  rats), normalized to sham-operated controls ( $n = 11$  rats). \* $P < 0.05$ , \*\*\* $P < 0.001$ , comparing sham to SCI; Mann-Whitney test. **(c)** Proportion of ~250-kDa and ~120-kDa bands relative to total Nav protein. \*\*\* $P < 0.001$ , comparing ~250-kDa and ~120-kDa bands; Mann-Whitney test. **(d)** Pan-Nav immunoblot in neonatal rats with SCI, treated with vehicle (dimethyl sulfoxide; DMSO) or MDL28170 (10 mg/kg/d for 8 d). One rat per lane. **(e)** Quantification of ~250-kDa and ~120-kDa bands in MDL28170-treated rats with SCI ( $n = 12$ ), normalized to vehicle-treated rats with SCI ( $n = 9$ ). \*\*\* $P < 0.001$ , comparing vehicle-treated rats to MDL28170-treated rats; Mann-Whitney test. **(f)** Proportion of the ~250-kDa and ~120-kDa bands normalized to total Nav protein. \*\*\* $P < 0.001$ , comparing ~250-kDa and ~120-kDa bands; Mann-Whitney test. **(g)** Leak-subtracted  $I_{NaP}$  from sham-operated rats ( $n = 60$  motoneurons), and vehicle-treated ( $n = 62$  motoneurons) and MDL28170-treated neonatal rats with SCI ( $n = 63$  motoneurons; 10 mg/kg/d for 8 d). **(h)** Threshold (left), amplitude (middle) and density (right) of  $I_{NaP}$ . \* $P < 0.05$ , \*\*\* $P < 0.001$ , one-way ANOVA. **(i)** TTX-sensitive, leak-subtracted  $I_{NaP}$  from Nav1.6-expressing HEK293 cells, a few minutes after internal perfusion with calpain (0.25  $\mu$ g/ml). **(j)** Comparison of time-course changes in the threshold (left) and amplitude (right) of  $I_{NaP}$  between untreated cells ( $n = 9$ ) and calpain-treated cells ( $n = 13$ ). \*\* $P < 0.01$ , \*\*\* $P < 0.001$ , repeated measures two-way ANOVA. Data are mean  $\pm$  s.e.m. for all panels.

protein (Fig. 2e,f). MDL28170 blocked the calpain-induced cleavage (Fig. 2e, right two bands). Similar results were obtained for Nav1.6 channels expressed in HEK293 cells. The application of calpain reduced the native ~250-kDa band to generate a lower molecular weight band of ~120 kDa ( $P < 0.01$ ; Fig. 2g,h). In sum,  $\alpha$ -subunits of Nav channels in the adult rat spinal cord, and specifically the Nav1.6 isoform that is prominently expressed in motoneurons, are substrates of calpains.

### Calpain is involved in SCI-induced potentiation of $I_{NaP}$

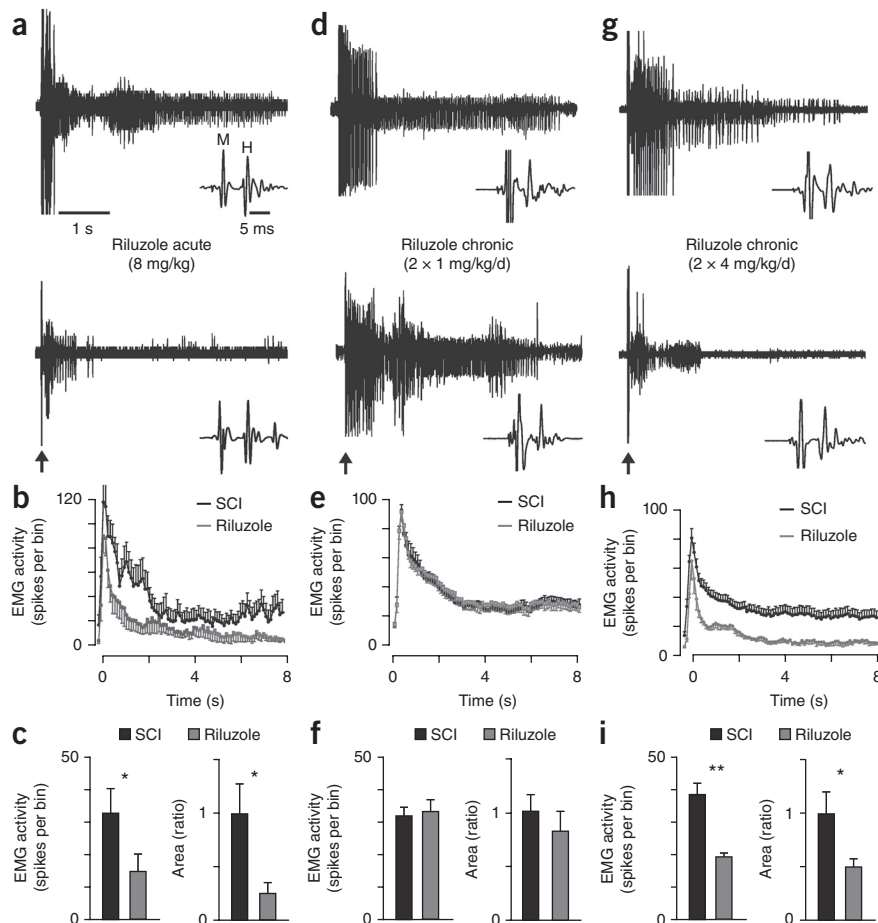
To further examine the role of calpain in the SCI-induced cleavage of Nav  $\alpha$ -subunits, we employed a SCI model in neonatal rats that, when compared to the adult model, more readily enables patch-clamp recordings to be obtained from motoneurons in acute spinal cord slices *in vitro*. SCI performed at birth induced a cleavage of Nav channels similar to what was observed after SCI in adults ( $P < 0.001$ ; Fig. 3a–c). Intraperitoneal (i.p.) injections of MDL28170 (10 mg/kg/d for 8 d, beginning 10 min after injury), which readily crosses the blood-brain barrier<sup>22</sup>, reduced the ~120-kDa band by  $45 \pm 6\%$  ( $P < 0.001$ ; Fig. 3d,e), as compared to vehicle-injected controls with SCI, but did not affect the ~250-kDa band ( $P > 0.05$ ; Fig. 3d,e), such that the relative proportions of the full-length and cleaved  $\alpha$ -subunits were reversed (Fig. 3f).



We performed voltage-clamp recordings to examine the biophysical properties of  $I_{NaP}$  in lumbar motoneurons. In response to slow voltage ramps, lumbar motoneurons displayed a large inward current (Fig. 3g), which we attributed to  $I_{NaP}$  because it was abolished by the known  $I_{NaP}$  inhibitors riluzole (5–10  $\mu$ M)<sup>14</sup> and tetrodotoxin (TTX) (1  $\mu$ M; Supplementary Fig. 2). SCI resulted in an upregulation of  $I_{NaP}$  (Fig. 3g)—characterized by a negative shift of the activation threshold—as well as an increase in both the absolute  $I_{NaP}$  current and the  $I_{NaP}$  current density, as compared to sham-operated controls ( $P < 0.001$ ; Fig. 3h). Chronic treatment of neonatal SCI-model rats with MDL28170 reduced the amplitude ( $P < 0.001$ ; Fig. 3g,h) and the density of  $I_{NaP}$ , as compared to rats with vehicle-treated SCI ( $P < 0.05$ ; Fig. 3h). Note that the biophysical properties of  $I_{NaP}$  recorded from motoneurons in sham-operated controls were similar in both untreated and MDL28170-treated animals (Supplementary Fig. 3).

Because our data suggested that the expression of Nav1.6, the major Nav channel isoform in motoneurons, is altered after SCI, we then specifically investigated calpain-mediated changes in the  $I_{NaP}$  that is mediated by Nav1.6 channels expressed in HEK293 cells.

**Figure 4** Riluzole decreases spasms in rats with SCI. **(a,d,g)** Representative EMG responses of the flexor digitorum brevis muscle (FDB), evoked by tibial nerve stimulation (arrows) in adult animals with SCI before (top) and after (bottom) acute i.p. administration of riluzole (8 mg/kg;  $n = 8$  rats; **a**) or chronic i.p. administration of riluzole twice a day for 2 weeks at 1 mg/kg ( $n = 7$  rats; **d**) or at 4 mg/kg ( $n = 8$  rats; **g**). Insets illustrate enlargements of the M wave and H reflex. **(b,e,h)** Average post-stimulus time histogram (PSTH; bin width, 100 ms) of FDB multiunit recordings collected before (black) and after (gray) the above-mentioned riluzole treatments. **(c,f,i)** Quantifications of PSTH, Number of spikes per bin (left) and area under the curve (right). \* $P < 0.05$ , \*\* $P < 0.01$  comparing animals before and after the riluzole treatments by a Mann-Whitney test. Data are mean  $\pm$  s.e.m. for all panels.



Intracellular dialysis of active calpain (0.25  $\mu$ g/ml) during voltage-clamp recordings produced a gradual hyperpolarization of the Nav1.6-mediated  $I_{NaP}$  activation threshold, which was not observed in untreated cells ( $P < 0.001$ ; **Fig. 3i,j**). Over the same 4-min recording duration,  $I_{NaP}$  amplitude increased in calpain-treated cells ( $P < 0.001$ ; **Fig. 3i,j**) and was abolished by TTX (1  $\mu$ M; **Fig. 3i**). The biophysical properties of  $I_{NaP}$  were stable when calpain was discarded from the intrapipette solution (**Fig. 3j** and **Supplementary Fig. 4**).

### Blocking $I_{NaP}$ reduces spasms in rats with chronic SCI

In awake adult rats with chronic SCI, we evoked hind-limb muscle spasms by stimulation of the tibial nerve, while simultaneously taking electromyography (EMG) recordings from the flexor digitorum brevis muscle. Responses were typically characterized by an intense muscle contraction, and were often followed by the self-sustained activity of motor units, with a mean discharge rate of  $14 \pm 1.6$  Hz (**Fig. 4a-c**). Nearly half of the motor units (13 of 28) fired below 10 Hz, a slow discharge thought to be driven by  $I_{NaP}$  (refs. 4,8,9,23–25). Next,

we monitored muscle spasms in the same rats with SCI both before and after the administration of riluzole, which is known to inhibit  $I_{NaP}$  (ref. 26). The initial muscle spasms were significantly reduced 60 min after a single i.p. injection of riluzole (8 mg/kg;  $P < 0.05$ ; **Fig. 4a-c**), and self-sustained activity of the motor units dropped in number to six, with a firing frequency above 10 Hz ( $21.2 \pm 3.1$  Hz). The effect was specific to long-lasting tonic activity, because the M wave and the monosynaptic Hoffmann reflex (H reflex) were not affected ( $P > 0.05$ ; **Fig. 4a** insets and **Supplementary Table 1**). We also monitored muscle spasms before and after chronic treatment with riluzole for 2 weeks in the same rats with SCI (beginning 30–90 d after injury). Although a low-dose riluzole treatment ( $2 \times 1$  mg/kg/d; i.p.) had no effect ( $P > 0.05$ ; **Fig. 4d-f**), rats treated with a higher dose

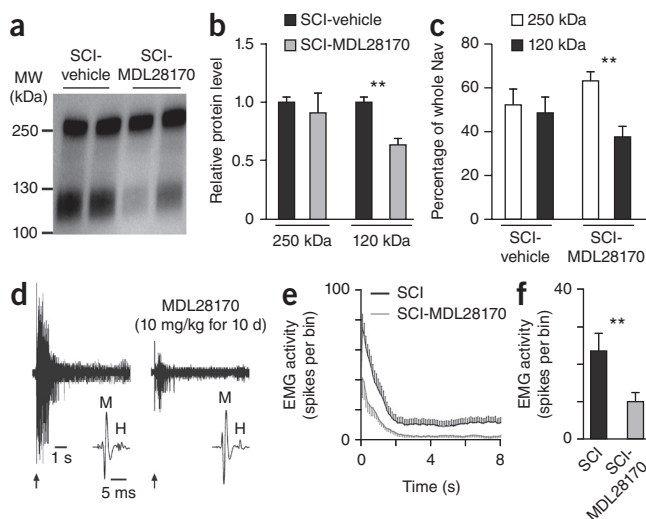
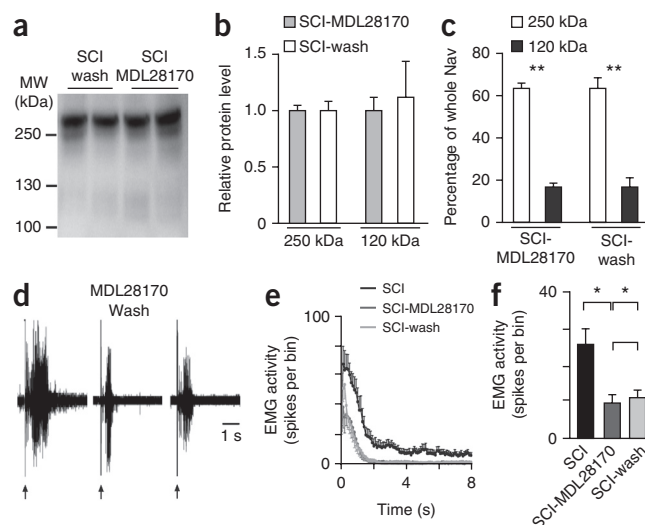


**Figure 5** Calpain inhibition restores Nav expression and decreases spasms in rats with SCI. **(a)** Pan-Nav immunoblot in adult rats with SCI (60 d after surgery) treated with vehicle or MDL28170 (10 mg/kg/d for 10 d). One rat per lane. **(b)** Quantification of immunoreactive ~250-kDa and ~120-kDa bands in MDL28170-treated rats with SCI ( $n = 7$ ; gray), normalized to SCI vehicle-treated rats ( $n = 5$ ; black). \*\* $P < 0.01$ , comparing vehicle-treated to MDL28170-treated rats; Mann-Whitney test. **(c)** Proportion of immunoreactive ~250-kDa and ~120-kDa bands, normalized to total Nav protein. \*\* $P < 0.01$ , comparing the ~250-kDa to the ~120-kDa band; Mann-Whitney test. **(d)** Representative EMG responses of the FDB muscle, evoked by stimulation of the tibial nerve (arrows) in adult rats with SCI ( $n = 10$ ) before (left) and after chronic treatment with MDL28170 (10 mg/kg/d for 10 d; right). **(e)** Average PSTH; bin width, 100 ms of FDB recordings before (black) and after (gray) chronic treatment with MDL28170. **(f)** Mean spikes per bin. \*\* $P < 0.01$ , before and after MDL28170 treatment; Mann-Whitney test. Data are mean  $\pm$  s.e.m. for all panels.

**Figure 6** Calpain inhibition has a long-lasting effect on the restoration of Nav expression and the reduction of spasms after SCI. **(a)** Pan-Nav immunoblot in adult MDL28170-treated rats with SCI (60 d after surgery) (10 mg/kg/d for 10 d) and tested either at the end of the 10 d treatment ( $n = 5$  rats (SCI-MDL28170)) or 3 weeks later ( $n = 6$  rats (SCI-wash)). **(b)** Quantification of immunoreactive ~250-kDa and ~120-kDa bands in SCI rats MDL28170-treated and tested 3 weeks after the discontinuation of the chronic treatment (SCI-wash), normalized to SCI rats treated with MDL28170 and tested at the end of the treatment (SCI-MDL28170).  $P > 0.05$ , comparing SCI-wash and SCI-MDL28170 rats; Mann-Whitney test. **(c)** Proportion of immunoreactive ~250-kDa and ~120-kDa bands, normalized to total Nav protein.  $**P < 0.01$ , comparing ~250-kDa to ~120-kDa bands; Mann-Whitney test. **(d)** Representative EMG responses of the FDB muscle, evoked by stimulation of the tibial nerve (arrows) in the same adult animals with SCI before (left) and after chronic i.p. administration of MDL28170 (10 mg/kg/d) for 10 d (middle), and 3 weeks after the discontinuation of the chronic treatment (right). **(e)** Average PSTH; bin width, 100 ms of FDB multiunit recordings collected before (black) and after chronic administration of MDL28170 (dark gray), and 3 weeks after the discontinuation of chronic treatment (wash; light gray). **(f)** Average number of spikes per bin in the PSTH.  $*P < 0.05$  comparing SCI, SCI-MDL28170 and SCI-wash groups by one-way ANOVA. Data are mean  $\pm$  s.e.m. for all panels.



( $2 \times 4$  mg/kg/d; i.p.) exhibited markedly reduced muscle spasms as compared to those measured before treatment ( $P < 0.01$ ; **Fig. 4g–i**), but showed no change in the M wave or H reflex (**Supplementary Table 1**). In high-dose riluzole-treated rats, very few motor units ( $n = 3$ ) continued to spike at a rate lower than 10 Hz. This beneficial effect was temporary; muscle spasms reappeared 2 weeks after the discontinuation of the chronic treatment (**Supplementary Fig. 5**).

#### Calpain inhibition prevents cleavage and reduces spasms in rats with chronic SCI

Finally, we investigated the effect of chronic treatment with MDL28170 in adult rats with chronic SCI. The animals were injected with MDL28170 (10 mg/kg/d; i.p.) or vehicle solution daily for 10 d, beginning 30–60 d after SCI. Such treatment reduced the cleavage of Nav (**Fig. 5a**), which we confirmed by the presence of a lower relative proportion of the ~120-kDa band in MDL28170-treated rats with SCI, as compared to vehicle-treated controls ( $P < 0.01$ ; **Fig. 5b**). The proportion of total Nav protein represented by the ~120-kDa band was smaller than that represented by the ~250-kDa band in MDL28170-treated rats with SCI, whereas the 120-kDa and ~250-kDa bands were found to represent roughly equal proportions in the vehicle-treated SCI control group ( $P < 0.01$ ; **Fig. 5c**). Furthermore, EMG responses recorded from the flexor digitorum brevis muscle were markedly reduced, as compared to those measured before treatment with MDL28170 in the same animals ( $P < 0.01$ ; **Fig. 5d–f**), whereas the M wave and H reflex were not affected (**Supplementary Table 2**). Chronic treatment with the vehicle did not change EMG responses (**Supplementary Fig. 6**). Remarkably, an additional reduction of EMG responses was observed after a single administration of riluzole (8 mg/kg; i.p.) in animals chronically treated with MDL28170 ( $P < 0.05$ ; **Supplementary Fig. 7**).

The long-lasting beneficial effect of chronic MDL28170 treatment was then tested on another set of animals (**Fig. 6**). Three weeks after the discontinuation of the 10 d treatment ('wash' animals), cleavage of Nav remained low (**Fig. 6a**), and the ~120-kDa band was similar to that observed at the end of the chronic treatment ( $P > 0.05$ ; **Fig. 6b**) and remained much smaller than the ~250-kDa band ( $P < 0.01$ ; **Fig. 6c**). Similarly, muscle spasms quantified at the end of the chronic treatment remained at similar levels when assayed

3 weeks later ( $P > 0.05$ ; **Fig. 6d–f**), and they were markedly reduced, as compared to those measured before treatment in the same animals ( $P < 0.05$ ; **Fig. 6d–f**). Finally, when we considered all rats for which both spasms and proteolysis had been assessed, a significant correlation was found between both parameters ( $P < 0.01$ ; **Supplementary Fig. 8**); i.e., rats with spasticity were those in which a prominent ~120-kDa band was expressed.

#### DISCUSSION

Here we demonstrate for the first time a long-lasting cleavage of Nav channels in the spinal cord after SCI, and we identify calpain as the factor responsible for this proteolysis. Proteolysis of Nav channels is associated with an upregulation of  $I_{NaP}$  in lumbar motoneurons. A clear relationship between these two events is given by our studies on HEK293 cells that express Nav1.6 channels, in which calpain-mediated cleavage of Nav1.6 was found to upregulate  $I_{NaP}$ . A similar relationship has been pointed out for epithelial sodium channels (ENaC)<sup>27</sup>. Indeed, the co-expression of a serine protease with ENaC in *Xenopus* oocytes increases the basal activity of the sodium channel by two- to threefold<sup>28</sup>. The tight relationship between the functionality of the channel and its proteolysis is further supported by the observation that internal perfusion of voltage-clamped squid axons with the proteolytic enzyme pronase prevents the inactivation of the sodium conductance and generates a pronounced  $I_{NaP}$  (ref. 29). Lastly, calpain inhibition decreases the late sodium current in ventricular cardiomyocytes that is associated with chronic heart failure<sup>30</sup>. We observed a similar effect in our study: MDL28170 treatment after SCI limited the enhancement of  $I_{NaP}$  in motoneurons. However, the rescue was partial, suggesting the existence of calpain-independent mechanism(s) involved in  $I_{NaP}$  upregulation. Given that the activation of 5-HT<sub>2</sub> receptors upregulates the  $I_{NaP}$  (ref. 4), the constitutive activation of 5-HT<sub>2</sub> receptors after SCI<sup>10</sup> might be one of these mechanisms. The Ca<sup>2+</sup> PIC of motoneurons is also facilitated by 5-HT<sub>2</sub> receptors<sup>31</sup> and their constitutive activity after SCI<sup>10</sup>. Because of the low Ca<sup>2+</sup>-buffering capacity of motoneurons<sup>32</sup>, an increase in the magnitude of the Ca<sup>2+</sup> PIC might activate Ca<sup>2+</sup>-dependent calpains. Then, calpains upregulate  $I_{NaP}$  not only by increasing its magnitude, but also by hyperpolarizing its activation threshold, such as has been reported in sacral motoneurons from adult rats with chronic SCI<sup>24</sup>. The enhancement of the  $I_{NaP}$  in turn increases the excitability of motoneurons<sup>15</sup> by facilitating: 1) the spike initiation

during slowly rising inputs<sup>33</sup>; 2) the related, sub-threshold membrane oscillations at the source of a slow, self-sustained spiking activity, which is associated with abnormally slow firing of motor units recorded in humans with spasticity<sup>4,8,9,23–25</sup>; and 3) the recruitment of the high-threshold  $\text{Ca}^{2+}$  PIC<sup>8,15</sup> that ultimately leads to the self-sustained firing associated with intense muscle spasms<sup>8,9</sup>. In this context, riluzole reduces spasticity by decoupling the tandem relationship of  $I_{\text{NaP}}$  and  $\text{Ca}^{2+}$  PIC.

Calpain proteolyzes the Nav1.2  $\alpha$ -subunit after a traumatic brain injury<sup>19,34</sup>. Proteolyzed Nav channels remain in the plasma membrane<sup>19</sup> and might account for the substantial increase seen in the expression of Nav1.6 channels in the AISs of motoneurons after SCI. Motoneurons alone are unlikely to account for all of the changes in the expression of Nav channels located below the lesion. Whereas no changes occur in Renshaw cells, increases in the expression of both Nav1.6 channels in the lumbar white matter<sup>35</sup> and Nav1.3 channels in dorsal horn neurons<sup>36</sup> have been described after SCI. Similarly, increases in the expression of Nav1.6 channels in microglia<sup>37</sup> might also arise after SCI. Calpain probably proteolyzes other substrates, in addition to Nav channels. Expression of the potassium-chloride co-transporter KCC2 was shown to be downregulated in motoneurons after SCI and to cause a net disinhibition, thereby contributing to the generation of spasticity<sup>3</sup>. It is worth mentioning that the C-terminal domain of KCC2 is sensitive to calpain, which alters its ability to extrude  $\text{Cl}^-$  ions<sup>38</sup>. This leads us to consider the possibility that a proteolytic cleavage of both the Nav channels and KCC2 may compose the upstream mechanism of spasticity.

Calpains exist as two major isoforms,  $\mu$ -calpain (or calpain 1) and m-calpain (or calpain 2), that differ from each other in the range of  $\text{Ca}^{2+}$  concentrations that they require for half-maximal activation ( $\mu\text{M}$  and  $\text{mM}$  ranges, respectively). The expression level of calpain markedly increases a few hours after SCI<sup>39–42</sup>, especially in motoneurons<sup>43</sup>. The activation of calpain 1, but not of calpain 2, contributes to initial reactive gliosis and tissue damage after SCI<sup>40,44,45</sup>, but calpain activity is confined to the injury site<sup>46</sup>. In regard to the calpain-mediated upregulation of  $I_{\text{NaP}}$ , this observation is compatible with the small  $I_{\text{NaP}}$  recorded in sacral motoneurons after acute SCI<sup>24</sup>. Although the increased expression of calpain during the acute phase of injury is well documented, very little is known about its expression during the chronic phase. However, global gene expression, as measured through laser capture of mRNA in sacral motoneurons below the SCI, showed differentially expressed genes encoding calpastatin (a natural inhibitor of calpains) and calpain 1 (ref. 47). In particular, expression of the gene encoding calpastatin decreases 21 d after SCI, whereas the gene encoding calpain 1 increases its expression 60 d after SCI. These data fit with a gradual activation of calpains in the spinal cord, in parallel with both the proteolytic cleavage of Nav channels and the emergence of spasticity in hind limbs. The isoform of calpain that is involved in the chronic phase of SCI should be investigated further in the future. It is worth mentioning that the expression of calpain 1, but not of calpain 2, was shown to be increased in the dorsal horn of the spinal cord 3–4 weeks after peripheral nerve ligation<sup>38</sup>.

The present study opens up new avenues for the treatment of spasticity after SCI. These strategies would consist of targeting  $I_{\text{NaP}}$  or the upstream mechanism, calpain-mediated proteolysis of Nav channels. The magnitude of  $I_{\text{NaP}}$  can be decreased by riluzole, which is currently licensed for the symptomatic treatment of amyotrophic lateral sclerosis (ALS). The therapeutic potential of riluzole has long been considered to be related mainly to an antiglutamatergic action<sup>48</sup>. However, the administration of riluzole reduced muscle spasms in

rats with SCI, without affecting the H reflex that results from the activation of glutamatergic  $I_a$  afferents, thereby demonstrating that the antiglutamatergic action of this drug could not account for the observed effects. The observed effect of riluzole probably results from an inhibition of  $I_{\text{NaP}}$ <sup>11,14</sup>, a current that was shown to be upregulated and to contribute to reflex hyperexcitability in the chronic phase of SCI in both rats<sup>8</sup> and humans<sup>49</sup>. In line with this assumption, the slow motor-unit activity ascribed to the regenerative activation of  $I_{\text{NaP}}$ <sup>4,8,9,23–25,50</sup> is almost silenced by riluzole. In further support of a role for riluzole in reducing spasticity, a dose of 8 mg/kg decreases the response of the tail muscles to cutaneous stimuli in rats with SCI at the sacral level<sup>51</sup>. Similarly, after SCI,  $I_{\text{NaP}}$  is upregulated in dorsal horn neurons<sup>52</sup>, and riluzole reduces neuropathic pain in rats with SCI<sup>53</sup>. All together, these data provide strong preclinical evidence for the translation of this treatment to humans during the chronic stage of SCI, a process that will probably be facilitated by a major clinical trial that is currently in progress to test the neuroprotective effects of riluzole in the acute phase of SCI<sup>54</sup>.

Proteases, and particularly calpains, represent important pharmacological targets for the treatment of different human pathologies<sup>55</sup>. In the present study, the use of MDL28170 demonstrates the potential benefits of calpain-specific therapies for the treatment of spasticity. Similarly, a single intraspinal microinjection of MDL28170 after SCI markedly improves both locomotion and pathological outcome<sup>56</sup>. One caveat to the specificity of MDL28170 is its activity against the lysosomal cysteine protease cathepsin B, although MDL28170 provides a 2.5-fold better affinity for calpains than for cathepsin B (refs. 57,58). A predominant effect of MDL28170 on calpains can be predicted, given that a minimal systemic dose of MDL28170 was used to reduce cysteine proteinase activity in the central nervous system (CNS)<sup>22,20</sup> and that inhibitors targeting cathepsin B do not prevent the cleavage of sodium channels<sup>19</sup>. In line with this, calpain inhibition with genetic tools provides neuroprotection in the acute phase of injuries<sup>44</sup>.

The other major result of the present study is that even when transient treatment with a calpain inhibitor starts only after spasticity has been established, spasms can still be reduced for a long-lasting period. The post-injury administration of calpain inhibitors for a short period seems to be a rational and feasible treatment for spasticity induced by SCI, without being detrimental to the physiological functions of calpains<sup>59</sup> over a long period of time. Because the co-administration of riluzole with MDL28170 further reduced muscle spasms, a transient inhibition of calpain, followed by a chronic blockade of  $I_{\text{NaP}}$ , might be even more efficient than either given alone for a functional recovery after SCI.

## METHODS

Methods and any associated references are available in the [online version of the paper](#).

*Note: Any Supplementary Information and Source Data files are available in the [online version of the paper](#).*

## ACKNOWLEDGMENTS

We dedicate this article to the memory of our dear colleague and friend Laurent Vinay, who passed away on 26 March 2015. Vinay was absolutely dedicated to science and, specifically, to the field of spinal cord research. Everyone who interacted with him was marked by his kindness, humanity and devotion. Vinay will leave a great void behind. This study was supported by the International Spinal Research Trust (to L.V.; STR110), the Fondation pour la Recherche Médicale (to L.V. and F.B.; DEQ20130326540) and the French Institut pour la Recherche sur la Moelle épinière et l'Encéphale (to F.B.). P.B. is supported by the French National

Institute of Health and Medical Research (INSERM). We thank the company NSrepair for their help in surgery and postoperative care. We thank A.J. Powell and M. Bird for providing us with the HEK293 cell line stably expressing Nav1.6 (GlaxoSmithKline, Stevenage, UK).

#### AUTHOR CONTRIBUTIONS

C.B. designed and performed the immunohistochemistry, western blot and surgery. V.P. performed *in vivo* experiments, contributed to *in vitro* experiments and to surgery. P.B. designed and performed *in vivo* experiments. S.L. performed cell culture and participated in immunohistochemistry and western blot. M.B. participated in some *in vitro* experiments. A.V.-L. contributed to surgery and postoperative care. L.V. provided valuable expertise in the field of SCI research. F.B. designed and supervised the whole project and contributed to the *in vitro* experiments. C.B., V.P., P.B., L.V. and F.B. analyzed data. L.V. and F.B. wrote the manuscript.

#### COMPETING FINANCIAL INTERESTS

The authors declare no competing financial interests.

Reprints and permissions information is available online at <http://www.nature.com/reprints/index.html>.

- Biering-Sørensen, F., Nielsen, J.B. & Klinge, K. Spasticity-assessment: a review. *Spinal Cord* **44**, 708–722 (2006).
- Boulenguez, P. & Vinay, L. Strategies to restore motor functions after spinal cord injury. *Curr. Opin. Neurobiol.* **19**, 587–600 (2009).
- Boulenguez, P. *et al.* Down-regulation of the potassium-chloride cotransporter KCC2 contributes to spasticity after spinal cord injury. *Nat. Med.* **16**, 302–307 (2010).
- Harvey, P.J., Li, X., Li, Y. & Bennett, D.J. 5-HT<sub>2</sub> receptor activation facilitates a persistent sodium current and repetitive firing in spinal motoneurons of rats with and without chronic spinal cord injury. *J. Neurophysiol.* **96**, 1158–1170 (2006).
- Li, X., Murray, K., Harvey, P.J., Ballou, E.W. & Bennett, D.J. Serotonin facilitates a persistent calcium current in motoneurons of rats with and without chronic spinal cord injury. *J. Neurophysiol.* **97**, 1236–1246 (2007).
- Heckman, C.J., Gorassini, M.A. & Bennett, D.J. Persistent inward currents in motoneuron dendrites: implications for motor output. *Muscle Nerve* **31**, 135–156 (2005).
- Houngaard, J., Hultborn, H., Jespersen, B. & Kiehn, O. Bistability of  $\alpha$ -motoneurons in the decerebrate cat and in the acute spinal cat after intravenous 5-hydroxytryptophan. *J. Physiol. (Lond.)* **405**, 345–367 (1988).
- Li, Y., Gorassini, M.A. & Bennett, D.J. Role of persistent sodium and calcium currents in motoneuron firing and spasticity in chronic spinal rats. *J. Neurophysiol.* **91**, 767–783 (2004).
- Gorassini, M.A., Knash, M.E., Harvey, P.J., Bennett, D.J. & Yang, J.F. Role of motoneurons in the generation of muscle spasms after spinal cord injury. *Brain* **127**, 2247–2258 (2004).
- Murray, K.C. *et al.* Recovery of motoneuron and locomotor function after spinal cord injury depends on constitutive activity in 5-HT<sub>2C</sub> receptors. *Nat. Med.* **16**, 694–700 (2010).
- Tazerart, S., Vinay, L. & Brocard, F. The persistent sodium current generates pacemaker activities in the central pattern generator for locomotion and regulates the locomotor rhythm. *J. Neurosci.* **28**, 8577–8589 (2008).
- Brocard, F. *et al.* Activity-dependent changes in extracellular Ca<sup>2+</sup> and K<sup>+</sup> reveal pacemakers in the spinal locomotor-related network. *Neuron* **77**, 1047–1054 (2013).
- Brocard, F., Tazerart, S. & Vinay, L. Do pacemakers drive the central pattern generator for locomotion in mammals? *Neuroscientist* **16**, 139–155 (2010).
- Tazerart, S., Viemari, J.C., Darbon, P., Vinay, L. & Brocard, F. Contribution of persistent sodium current to locomotor pattern generation in neonatal rats. *J. Neurophysiol.* **98**, 613–628 (2007).
- Bouhadfane, M., Tazerart, S., Moqrish, A., Vinay, L. & Brocard, F. Sodium-mediated plateau potentials in lumbar motoneurons of neonatal rats. *J. Neurosci.* **33**, 15626–15641 (2013).
- Fukuoka, T., Kobayashi, K. & Noguchi, K. Laminae-specific distribution of alpha-subunits of voltage-gated sodium channels in the adult rat spinal cord. *Neuroscience* **169**, 994–1006 (2010).
- Duflocq, A., Le Bras, B., Bullier, E., Couraud, F. & Davenne, M. Nav1.1 is predominantly expressed in nodes of Ranvier and axon initial segments. *Mol. Cell. Neurosci.* **39**, 180–192 (2008).
- Croall, D.E. & Ersfeld, K. The calpains: modular designs and functional diversity. *Genome Biol.* **8**, 218 (2007).
- von Reyn, C.R. *et al.* Calpain mediates proteolysis of the voltage-gated sodium channel  $\alpha$ -subunit. *J. Neurosci.* **29**, 10350–10356 (2009).
- Kunz, S. *et al.* The calpain inhibitor MDL 28170 prevents inflammation-induced neurofilament light chain breakdown in the spinal cord and reduces thermal hyperalgesia. *Pain* **110**, 409–418 (2004).
- Arataki, S. *et al.* Calpain inhibitors prevent neuronal cell death and ameliorate motor disturbances after compression-induced spinal cord injury in rats. *J. Neurotrauma* **22**, 398–406 (2005).
- Markgraf, C.G. *et al.* Six-hour window of opportunity for calpain inhibition in focal cerebral ischemia in rats. *Stroke* **29**, 152–158 (1998).
- Harvey, P.J., Li, X., Li, Y. & Bennett, D.J. Endogenous monoamine receptor activation is essential for enabling persistent sodium currents and repetitive firing in rat spinal motoneurons. *J. Neurophysiol.* **96**, 1171–1186 (2006).
- Harvey, P.J., Li, Y., Li, X. & Bennett, D.J. Persistent sodium currents and repetitive firing in motoneurons of the sacrocaudal spinal cord of adult rats. *J. Neurophysiol.* **96**, 1141–1157 (2006).
- Li, Y. & Bennett, D.J. Persistent sodium and calcium currents cause plateau potentials in motoneurons of chronic spinal rats. *J. Neurophysiol.* **90**, 857–869 (2003).
- Urbani, A. & Belluzzi, O. Riluzole inhibits the persistent sodium current in mammalian CNS neurons. *Eur. J. Neurosci.* **12**, 3567–3574 (2000).
- Svenningsen, P. *et al.* Physiological regulation of epithelial sodium channel by proteolysis. *Curr. Opin. Nephrol. Hypertens.* **20**, 529–533 (2011).
- Vallet, V., Chraïbi, A., Gaeggeler, H.P., Horisberger, J.D. & Rossier, B.C. An epithelial serine protease activates the amiloride-sensitive sodium channel. *Nature* **389**, 607–610 (1997).
- Armstrong, C.M., Bezanilla, F. & Rojas, E. Destruction of sodium conductance inactivation in squid axons perfused with pronase. *J. Gen. Physiol.* **62**, 375–391 (1973).
- Undrovinas, A., Maltsev, V.A. & Sabbah, H.N. Calpain inhibition reduces amplitude and accelerates decay of the late sodium current in ventricular myocytes from dogs with chronic heart failure. *PLoS One* **8**, e54436 (2013).
- Murray, K.C., Stephens, M.J., Ballou, E.W., Heckman, C.J. & Bennett, D.J. Motoneuron excitability and muscle spasms are regulated by 5-HT<sub>2B</sub> and 5-HT<sub>2C</sub> receptor activity. *J. Neurophysiol.* **105**, 731–748 (2011).
- Palecek, J., Lips, M.B. & Keller, B.U. Calcium dynamics and buffering in motoneurons of the mouse spinal cord. *J. Physiol. (Lond.)* **520**, 485–502 (1999).
- Kuo, J.J., Lee, R.H., Zhang, L. & Heckman, C.J. Essential role of the persistent sodium current in spike initiation during slowly rising inputs in mouse spinal neurons. *J. Physiol. (Lond.)* **574**, 819–834 (2006).
- Schoch, K.M. *et al.* Brain injury-induced proteolysis is reduced in a novel calpastatin-overexpressing transgenic mouse. *J. Neurochem.* **125**, 909–920 (2013).
- Hunanyan, A.S. *et al.* Alterations of action potentials and the localization of Nav1.6 sodium channels in spared axons after hemisection injury of the spinal cord in adult rats. *J. Neurophysiol.* **105**, 1033–1044 (2011).
- Hains, B.C. & Waxman, S.G. Sodium channel expression and the molecular pathophysiology of pain after SCI. *Prog. Brain Res.* **161**, 195–203 (2007).
- Craner, M.J. *et al.* Sodium channels contribute to microglia/macrophage activation and function in EAE and MS. *Glia* **49**, 220–229 (2005).
- Zhou, H.Y. *et al.* N-methyl-D-aspartate receptor- and calpain-mediated proteolytic cleavage of K<sup>+</sup>-Cl<sup>-</sup> cotransporter-2 impairs spinal chloride homeostasis in neuropathic pain. *J. Biol. Chem.* **287**, 33853–33864 (2012).
- Banik, N.L., Matzelle, D.C., Gantt-Wilford, G., Osborne, A. & Hogan, E.L. Increased calpain content and progressive degradation of neurofilament protein in spinal cord injury. *Brain Res.* **752**, 301–306 (1997).
- Springer, J.E., Azbill, R.D., Kennedy, S.E., George, J. & Geddes, J.W. Rapid calpain I activation and cytoskeletal protein degradation following traumatic spinal cord injury: attenuation with riluzole pretreatment. *J. Neurochem.* **69**, 1592–1600 (1997).
- Schumacher, P.A., Eubanks, J.H. & Fehlings, M.G. Increased calpain I-mediated proteolysis, and preferential loss of dephosphorylated NF200, following traumatic spinal cord injury. *Neuroscience* **91**, 733–744 (1999).
- Ray, S.K. *et al.* Calpain activity and translational expression increased in spinal cord injury. *Brain Res.* **816**, 375–380 (1999).
- Li, Z., Hogan, E.L. & Banik, N.L. Role of calpain in spinal cord injury: increased calpain immunoreactivity in rat spinal cord after impact trauma. *Neurochem. Res.* **21**, 441–448 (1996).
- Yu, C.G. *et al.* Calpain 1 knockdown improves tissue sparing and functional outcomes after spinal cord injury in rats. *J. Neurotrauma* **30**, 427–433 (2013).
- Du, S. *et al.* Calcium influx and activation of calpain I mediate acute reactive gliosis in injured spinal cord. *Exp. Neurol.* **157**, 96–105 (1999).
- Shields, D.C., Schaefer, K.E., Hogan, E.L. & Banik, N.L. Calpain activity and expression increased in activated glial and inflammatory cells in penumbra of spinal cord injury lesion. *J. Neurosci. Res.* **61**, 146–150 (2000).
- Wienecke, J., Westerdahl, A.C., Hultborn, H., Kiehn, O. & Ryge, J. Global gene expression analysis of rodent motor neurons following spinal cord injury associates molecular mechanisms with development of postinjury spasticity. *J. Neurophysiol.* **103**, 761–778 (2010).
- Cifra, A., Mazzone, G.L. & Nistri, A. Riluzole: what it does to spinal and brainstem neurons and how it does it. *Neuroscientist* **19**, 137–144 (2013).
- Theiss, R.D., Hornby, T.G., Rymer, W.Z. & Schmit, B.D. Riluzole decreases flexion withdrawal reflex but not voluntary ankle torque in human chronic spinal cord injury. *J. Neurophysiol.* **105**, 2781–2790 (2011).
- Zijewind, I. & Thomas, C.K. Firing patterns of spontaneously active motor units in spinal cord-injured subjects. *J. Physiol. (Lond.)* **590**, 1683–1697 (2012).
- Kitzman, P.H. Effectiveness of riluzole in suppressing spasticity in the spinal cord injured rat. *Neurosci. Lett.* **455**, 150–153 (2009).
- Lampert, A., Hains, B.C. & Waxman, S.G. Upregulation of persistent and ramp sodium current in dorsal horn neurons after spinal cord injury. *Exp. Brain Res.* **174**, 660–666 (2006).
- Hama, A. & Sagen, J. Antinociceptive effect of riluzole in rats with neuropathic spinal cord injury pain. *J. Neurotrauma* **28**, 127–134 (2011).
- Grossman, R.G. *et al.* A prospective, multicenter, phase I matched-comparison group trial of safety, pharmacokinetics, and preliminary efficacy of riluzole in patients with traumatic spinal cord injury. *J. Neurotrauma* **31**, 239–255 (2014).

## ARTICLES

55. Ray, S.K. & Banik, N.L. Calpain and its involvement in the pathophysiology of CNS injuries and diseases: therapeutic potential of calpain inhibitors for prevention of neurodegeneration. *Curr. Drug Targets CNS Neurol. Disord.* **2**, 173–189 (2003).
56. Yu, C.G., Joshi, A. & Geddes, J.W. Intraspinal MDL28170 microinjection improves functional and pathological outcome following spinal cord injury. *J. Neurotrauma* **25**, 833–840 (2008).
57. Wang, K.K. Developing selective inhibitors of calpain. *Trends Pharmacol. Sci.* **11**, 139–142 (1990).
58. Mehdi, S. Cell-penetrating inhibitors of calpain. *Trends Biochem. Sci.* **16**, 150–153 (1991).
59. Goll, D.E., Thompson, V.F., Li, H., Wei, W. & Cong, J. The calpain system. *Physiol. Rev.* **83**, 731–801 (2003).



## ONLINE METHODS

**Animal care.** Wistar rats were housed under a 12 h light-dark cycle in a temperature-controlled area with *ad libitum* access to water and food. All animal care and use conformed to the French regulations (Décret 2010-118) and were approved by the local ethics committee CEEA 71-Comité d'éthique en neurosciences - INT Marseille (authorization Nb A9 01 13).

**Surgery and postoperative care.** Spinal cord transection was performed in adult and neonatal rats. Adult female Wistar rats (220–280g) were anesthetized with ketamine (Imalgen, Merial, 50 mg/kg i.p.) and medetomidine (Domitor, Janssen, 0.25 mg/kg i.p.) and treated preventively with a long-acting antibiotic (amoxicillin, Duphamox LA, Pfizer, 100 mg/kg subcutaneously (s.c.)). A mid-line skin incision was performed, and a local anesthetic (Procaine chlorhydrate 2%, Pharmy H) was injected into the paravertebral muscles before retraction. A laminectomy of the T8 dorsal vertebra was performed carefully to expose the spinal cord. After cutting the dura, the spinal cord was completely transected with small scissors at the T9 segmental level under local anesthesia. The paravertebral muscles and skin were then sutured and disinfected. The rats were rehydrated with 5 ml of 0.9% NaCl s.c. and kept warm in an incubator. Two hours later, they were awakened with an intramuscular (i.m.) injection of atipamezol (Antisedan, Janssen, 0.12 mg/kg) and with a morphinic analgesic s.c. injected (buprenorphine, Vetergesic, Sogeval, 0.05 mg/kg; three injections at 8 h intervals to cover the first 24 h). Rats were then placed in a warm room in clean individual cages with easily accessible, completely natural food for rats (Vitakraft) and water bottles containing 1.33 g/l of aspirin for 3 d (Aspégic nourisson, Sanofi Aventis). Their bladders were emptied twice a day until recovery of autonomy. Their water intake, temperature and weight were checked every day until they recovered an ascending weight curve. After 7 d, they were housed again with their initial cage partners. Occasional urinary infections were treated with enrofloxacin (Baytril, Bayer, 5 mg/kg/j for 3 d). In neonates (P0), the procedure was similar, except that animals were anesthetized by hypothermia, and after the complete transection of the spinal cord at the T8–T9 level, the lesion cavity was filled with sterile, absorbable, local hemostat Surgicoll. The wound was then covered with Steri-Strips (3M Health Care, St. Paul, Minnesota) and animals were kept warm and wet for 2 h in cotton-wool swab infused with their mother's smell, after which they were returned to their home cages with their mother. The antibiotic amoxicillin (150 mg/kg s.c.) was injected postoperatively. Sham-operated animals were subjected to all procedures except the spinal cord transection.

**Drug-treatment design.** Two main types of experimental treatments were performed. For treatment one, adult rats with SCI and chronic spasticity were randomly treated with either a single administration of riluzole (Riluzole-HCl, Tocris, 8 mg/kg i.p. diluted in phosphate-buffered saline (PBS) with 5% or 10% cyclodextrine; final pH corrected to 7.5) or vehicle 1 h before electrophysiological tests, or a twice daily i.p. administration of riluzole (1 mg/kg or 4 mg/kg) for 2 weeks, ending 15–24 h before the tests. A dose of 8 mg/kg was chosen for acute and chronic (2 × 4 mg/d) administration in rats with SCI, because the pharmacokinetic profile of this dose has been well characterized in rats with SCI<sup>60</sup>, and it is within the human-equivalent dose (HED) used for subjects, according to the power equation from the US Food and Drug Administration (FDA) Guidance for Industry (2005): HED = animal dose (mg/kg) × (animal wt/human wt in kg)<sup>0.33</sup>. For treatment two, the calpain inhibitor MDL28170 was administered once a day in spinal rats (10 mg/kg/d i.p., diluted in dimethyl sulfoxide (DMSO)), for 6–8 d in neonates and for 10 d in adults, beginning 30–60 d after injury, and control animals were injected with the vehicle only. The systemic administration of 10 mg/kg was used because it has been reported to be the minimal effective dose to produce a substantial inhibition of cysteine proteinase activity in the CNS<sup>20,22</sup>. The drug-administration paradigm comes from Arataki's study<sup>21</sup>, in which a daily i.p. injection of MDL28170 (10 mg/kg for 1 week) improved locomotor function after SCI. Treatments were administered by the experimenter in a blind manner.

**Electrophysiological assessment of spasticity in awake spinal rats.** Adult animals were tested 4–12 weeks after SCI, once all signs of spasticity were firmly established (excessive muscle tone, spasms and hyperreflexia); rats without spasticity after SCI were excluded. Rats with spasticity after SCI were progressively

habituated with an appetizing reward to be individually confined in a plexiglass tube and to have their paralyzed hind limbs immobilized with tape. For electrophysiological assessment of spasticity, a pair of stainless-steel stimulating needle electrodes was inserted transcutaneously into the surroundings of the tibial nerve above the ankle. A recording electrode was inserted percutaneously into the FDB (flexor of the lateral four toes), and the reference electrode was placed s.c. into the foot. The ground was s.c. at the base of the tail. Given that the rats were spinalized, they could not feel any pain when these needle electrodes were placed in their hindquarters. EMG signals were amplified (100×) and band-pass filtered (300 Hz to 5 kHz; A-M Systems Amplifier, Everett, Washington; model 1700) before sampling at 13.5 kHz (Digidata 1440A, Molecular Devices). After a 20 min acclimation period in the confinement tube, the tibial nerve was stimulated by using square pulses with increasing stimulus intensities (0.1 mA increments starting from 0.1 mA, 0.2 Hz, 0.2 ms; A-M systems stimulator, Model 2100) to obtain H-reflex and M-wave recruitment curves. A supramaximal single-pulse stimulation to elicit muscle spasms was then fixed throughout the experiment (two or three times the threshold intensity for the M wave), with 90 s interstimulus intervals.

**In vitro preparations and intracellular recordings.** Rat lumbar spinal cords were isolated at the end of the first postnatal week in ice-cold (<4 °C) artificial cerebrospinal fluid (aCSF) solution with the following composition (in mM): 232 sucrose, 3 KCl, 1.25 KH<sub>2</sub>PO<sub>4</sub>, 4 MgSO<sub>4</sub>, 0.2 CaCl<sub>2</sub>, 26 NaHCO<sub>3</sub>, 25 D-glucose, pH 7.4. The lumbar spinal cord was then introduced into a 1% agar solution, quickly cooled, mounted in a vibrating microtome (Leica VT1000S) and sliced (350 μm) through the L4–L5 lumbar segments. Slices were immediately transferred into the holding chamber, which was filled with aCSF composed of (in mM): 120 NaCl, 3 KCl, 1.25 NaH<sub>2</sub>PO<sub>4</sub>, 1.3 MgSO<sub>4</sub>, 1.2 CaCl<sub>2</sub>, 25 NaHCO<sub>3</sub>, 20 D-glucose, pH 7.4. All solutions were oxygenated with 95% O<sub>2</sub> and 5% CO<sub>2</sub>. Slices were visualized with infrared differential interference contrast (IR-DIC) microscopy by using a Nikon Eclipse E600FN upright microscope coupled with a 40× water-immersion lens. The image was enhanced with a Hitachi KP-200/201 infrared-sensitive CCD camera and displayed on a video monitor. Whole-cell patch-clamp recordings were performed with a Multiclamp 700B amplifier (Molecular Devices) on motoneurons located in the lateral ventral horn and were visually identified on the basis of their large soma. Only neurons with a membrane capacitance higher than 100 pF were considered. Patch electrodes (2–4 MΩ) were pulled from borosilicate glass capillaries (1.5 mm OD, 1.12 mm ID; World Precision Instruments) on a Sutter P-97 puller (Sutter Instruments Company) and filled with intracellular solution containing (in mM): 140 K<sup>+</sup>-gluconate, 5 NaCl, 2 MgCl<sub>2</sub>, 10 HEPES, 0.5 ethylene glycol tetraacetic acid (EGTA), 2 ATP, 0.4 GTP, pH 7.3 (280–290 mOsm). Pipette and neuronal capacitive currents were canceled, and after breakthrough, the series resistance was compensated and monitored. Recordings were digitized online and filtered at 10 kHz (Digidata 1322A, Molecular Devices). Whole-cell sodium currents were recorded with an aCSF composed of the following (in mM): 100 NaCl, 3 KCl, 1.25 NaH<sub>2</sub>PO<sub>4</sub>, 1.3 MgSO<sub>4</sub>, 3.6 MgCl<sub>2</sub>, 1.2 CaCl<sub>2</sub>, 25 NaHCO<sub>3</sub>, 40 D-glucose, 10 TEA-Cl, 0.1 CdCl<sub>2</sub>, pH 7.4 (31–32 °C). The main characterization of I<sub>NaP</sub> was accomplished by slow ramp increase from –70 mV to –10 mV, slow enough (12 mV/s) to prevent transient sodium channel opening.

**Stable mammalian cell line expressing Nav1.6 and intracellular recordings.** The HEK293 cells stably expressing hNav1.6 were grown to confluence at 37 °C with 5% CO<sub>2</sub> and plated on 100 mm-diameter petri dishes or in 175 cm<sup>2</sup> flasks in Dulbecco's modified Eagle's medium (DMEM) with Nutrient mixture F-12 supplemented with fetal bovine serum (FBS; 10%), L-glutamine (2 mM), penicillin (100 U/ml) and streptomycin (10 mg/ml; Life Technologies). G418 (0.4 mg/ml; Life Technologies) was added to select Nav1.6-expressing cells. Whole-cell sodium currents were recorded from HEK293 cells with an aCSF composed of the following (in mM): 110 NaCl, 3 KCl, 1 MgCl<sub>2</sub>, 1 CaCl<sub>2</sub>, 20 TEA, 5 CsCl, 10 HEPES, 11 glucose at pH 7.4 (23 °C). The main characterization of I<sub>NaP</sub> was accomplished by slow ramp increase from –100 mV to 90 mV. Patch electrodes (2–4 MΩ) were filled with intracellular solution containing (in mM): 100 CsCl, 30 K<sup>+</sup>-gluconate 5 NaCl, 2 MgCl<sub>2</sub>, 0.5 EGTA, 10 HEPES, 2 ATP, 0.4 GTP at pH 7.3. In some experiments, active calpain 1 (0.25 μg/ml; Abcam) was added to the intrapipette solution.

**Immunohistochemistry.** Transverse spinal cord sections at the lumbar L4–L5 level (20  $\mu\text{m}$  thick) were processed for immunohistochemistry using antibodies against Nav-channel isoforms (Pan, Nav1.1 and Nav1.6)<sup>17</sup>. For tissue preparations, adult rats were perfused transcardially with 1% paraformaldehyde (PFA) in PBS at 4 °C. Tissues were post-fixed for 1 h in 1% PFA at 4 °C and cryoprotected overnight in 20% sucrose in PBS at 4 °C. Neonate spinal cords were dissected out, immersion-fixed for 1 h in 0.25% PFA, washed in PBS and cryoprotected overnight at 4 °C in 20% sucrose in PBS. Adult and neonate lumbar spinal cords (L4–L5) were then frozen in Optimal Cutting Temperature (OCT) medium (Tissue Tec), cryosectioned (20  $\mu\text{m}$ ) and processed for immunohistochemistry. Sections from the control rats and rats with SCI were mounted on the same slides and processed simultaneously. Slices were then (i) rehydrated in PBS at room temperature (15 min); (ii) permeated with 1% bovine serum albumin (BSA), 2% natural goat serum (NGS) and 0.2% Triton x-100 (1 h); (iii) incubated overnight at 4 °C in the following affinity-purified rabbit Nav1.1 (residues 465–481; 1:400; AB5204, Merck-Millipore), Nav1.6 (residues 1042–1061; 1:200; ASC009, Alomone)-specific polyclonal antibodies, mouse pan-Nav (preserved sequence of the intracellular III–IV loop; 1:500; clone K58/35, Sigma-Aldrich) or gephyrin (mAb7a, 1:400; Synaptic System) specific monoclonal antibodies; (iv) washed in PBS (3  $\times$  5 min); (v) subjected to an additional overnight incubation with the second primary antibody for double immunostaining and then washed again in PBS (3  $\times$  5 min); (vi) incubated with fluorescent-conjugated secondary antibodies (Alexa 488- or 633-conjugated mouse- or rabbit-specific antibodies (1:800 and 1:400; Life Technologies) that were used for visualization of the mouse monoclonal or rabbit polyclonal antibodies, respectively, in a solution containing 1% BSA and 2% NGS (1.5 h); (vii) washed in PBS 3  $\times$  5 min; (viii) coverslipped with a gelatinous aqueous medium. In control experiments, the primary antiserum was either omitted or replaced with rabbit or mouse immunoglobulin fraction during the staining protocol. Images were taken with the confocal microscope Olympus FV500 at 20 $\times$  and 60 $\times$  magnification, digitized in stacks of 0.2–1  $\mu\text{m}$ -thick optical sections and processed with the FluoView (Olympus) software. Each figure corresponds to a projection image from a stack of optical sections.

**Membrane-protein isolation and western blots.** Tissues were collected from spinal cord lumbar enlargements and frozen after removing the dorsal and ventral roots. For the membrane fraction, corresponding to the plasma membrane-enriched fraction, samples were homogenized in ice-cold lysis buffer (320 mM sucrose, 5 mM Tris-HCL pH 7.5, 10  $\mu\text{M}$  iodoacetamide) supplemented with protease inhibitors (CompleteMini, Roche diagnostic, Basel, Switzerland). Unsolubilized material was pelleted by centrifugation at 7,000g for 5 min. The supernatant was subjected to an additional centrifugation step at 18,000g for 70 min at 4 °C. Pellets were collected and homogenized in ice-cold lysis buffer (1% Igepal CA-630, PBS 1X, 0.1% SDS, 10  $\mu\text{M}$  iodoacetamide), supplemented with protease inhibitors (CompleteMini, Roche diagnostic). Protein concentrations were determined by using a detergent-compatible protein assay (Bio-Rad). Equal protein amounts (60  $\mu\text{g}$ ) from samples were size fractionated by 6% (vol/vol) SDS/PAGE from 40% Acryl/Bisacrylamide (29/1) commercial solution, transferred to a polyvinylidene fluoride (PVDF) membrane and probed with the sodium channel  $\alpha$ -subunit III–IV loop (pan:Sigma-Aldrich; 1:500) antibody at 4 °C overnight in Tris-buffered saline containing 5% fat-free milk powder. The blot was then incubated for 1 h at 22 °C with an ImmunoPure goat HRP-conjugated mouse-specific antibody (1:40,000 in blocking solution; Thermo Scientific). The proteins were blotted with the substrate HRP immobilon Western (Merck-Millipore). Signal intensities were measured with the image-analysis software Quantity-One (Bio-Rad).

**Calpain-cleavage assay.** *In spinal cord membrane preparations.* Lumbar spinal cords were homogenized in 400  $\mu\text{l}$  sucrose buffer for membrane preparation (300 mM sucrose, 10 mM Tris base, 2 mM EDTA, 0.5 mM PMSF and 1  $\mu\text{M}$  pepstatin A) and centrifuged at 7,000g for 5 min at 4 °C. The supernatant was subjected to an additional centrifugation step at 18,000g for 70 min at 4 °C, and the pellet was resuspended in the same buffer. Protein concentrations were analyzed using the Bio-Rad Dc Protein Assay. Membrane preparations were then pretreated with or without the calpain inhibitor (30  $\mu\text{M}$  MDL28170, Calbiochem) for 15 min on ice. Calcium (2–10 mM  $\text{CaCl}_2$ ) and/or calpain 1

(0.5–3 U, Calbiochem) were added for 15 min at room temperature (24 °C). The reaction was stopped after the addition of the electrophoresis sample buffer.

*In spinal cord total preparations.* For the assay activation of endogenous calpain, part of the homogenate obtained after lysis sucrose buffer was solubilized in lysis buffer (1/1) containing 1% Igepal CA-630, 0.1% SDS, PBS 1 $\times$ , 5 mM EDTA, 0.5 mM PMSF and 1  $\mu\text{M}$  pepstatin A, pH 7.4, and centrifuged at 18,000g for 30 min at 4 °C. The supernatant was collected. The total preparations were pretreated with or without the calpain inhibitor (30  $\mu\text{M}$  MDL 28270, Calbiochem) for 15 min on ice. Calcium (10 mM  $\text{CaCl}_2$ ) was added or not for 15 min at 24 °C. The reaction was stopped after the addition of the electrophoresis sample buffer.

*In HEK293 cell line stably expressing hNav<sub>1.6</sub>.* Calpain-cleavage assay processing was similar to that described above, with an additional step for cell detachment without trypsin.

**Statistical and data analysis.** The sample size was estimated considering the variation and mean of the samples. No statistical method was used to predetermine sample size. Adult animals were tested 4–12 weeks after SCI, when signs of spasticity were firmly established; rats without spasticity were excluded. Rats with spasticity were randomly assigned to groups for studies *in vivo*. Treatments were administered by the experimenter in a blind manner. Group outcome assessment was also done in a blinded manner. Group measurements were expressed as means  $\pm$  s.e.m. We used Mann-Whitney tests and one- or two-way ANOVA tests with or without repeated measures as appropriate (GraphPad Prism 5 software). For all statistical analyses, the data met the assumptions of the test, and the variance between the statistically compared groups was similar. Significance was set at  $P < 0.05$ . All analyses were performed blind for the treatments.

**Immunohistochemistry.** Sections were scanned using a laser-scanning confocal microscope in stacks of 1  $\mu\text{m}$ -thick optical sections at 20 $\times$  magnification. Each optical section resulted from two scanning averages. We used identical settings, which were finely tuned to avoid saturation, for the whole series. Quantification of Nav<sub>1.6</sub> and Pan staining intensities were performed using the FluoView Software (version 5, Olympus). Measurements were performed on AISs from the motoneurons identified as the biggest cells located in the ventral horn. AISs from motoneurons were identified as large linear structures double labeled by Pan- and Nav1.6-specific antibodies, located within the ventral horn and for which the beginning and the end of the structure could be clearly determined (>10  $\mu\text{m}$  in length), excluding nodes of Ranvier. The mean pixel intensities of Pan- and Nav1.6-specific fluorescence were measured by tracing the labeled AISs using the multipoint line feature of the FluoView software (see Fig. 1a, inset). Each value was then normalized to the mean value measured from sections of sham-operated rats on the same slide. The measurements were repeated with similar numbers of motoneurons per animal. Similar quantification was performed on the thin AISs from Renshaw cells identified by characteristic intense, very large and abundant gephyrin clusters on the proximal dendrites and soma located in the most ventral area of spinal cord lamina VII. As a negative control, we replaced the primary antibody with a normal rabbit or mouse immunoglobulin fraction (same amount) and observed a complete absence of labeling in AISs.

**Extracellular recordings.** The amplitudes of the evoked M waves and H reflexes were measured using the area under the curve, including the first main two peaks of each wave after rectification of the signals. The maximal M response ( $M_{\text{max}}$ ), representing the activation of the total motoneuronal pool by a maximal stimulus, was used for data normalization within and between animals. Evoked, long-lasting reflexes were quantified from rectified digital signals by measuring the area under the curve from the end of the monosynaptic reflex until the first 4 s recordings. Note that the background area was previously subtracted. These areas were divided by the corresponding  $M_{\text{max}}$  area, and normalized in the final histogram to the mean value of the vehicle-treated group (Fig. 4c,f,i, right). PSTHs were also calculated for the whole spike trains by using a voltage-peak detector with time bins of 100 ms. Finally, by means of a motor-unit decomposition algorithm (Clampfit software, Molecular Devices), we isolated motor units that fire repetitively during a stationary period of the EMG recording. By setting an amplitude threshold, single motor-unit action potentials were selected offline. Each selected potential was then visually checked, and we verified that they were of similar shape and belonged to the same motor unit.

Once all units were selected for a single trial, they were superimposed to compare the shape of each potential and to examine how it changed throughout a recording trial. The motor-unit discharge frequency was taken as the mean rate calculated during a stationary period of discharge. Only units still firing 4 s after the stimulation were considered to be sustained-firing motor units.

*Intracellular recordings.* Only cells that exhibited a holding membrane potential and an action potential amplitude larger than 45 mV were considered. The junction potential was corrected offline on the basis of the composition of the internal and external solutions used for recordings. We defined the voltage-dependent

activation threshold of the  $I_{\text{NaP}}$  as the membrane potential at which the slope of leak-subtracted current becomes negative. We measured the magnitude of the  $I_{\text{NaP}}$  by looking at the peak of the leak-subtracted inward current during the ascending phase of the voltage command. For current-density measurements, currents were divided by the cell capacitance, as read from the amplifier.

60. Wu, Y. *et al.* Delayed post-injury administration of riluzole is neuroprotective in a preclinical rodent model of cervical spinal cord injury. *J. Neurotrauma* **30**, 441–452 (2013).